Magnetic circular dichroism in real-time time-dependent density functional theory

K.-M. Lee,[1] K. Yabana,[1,2] and G. F. Bertsch[3,a]

[1]*Graduate School of Pure and Applied Sciences, University of Tsukuba, Tsukuba 305-8571, Japan*
[2]*Center for Computational Sciences, University of Tsukuba, Tsukuba 305-8571, Japan*
[3]*Institute for Nuclear Theory and Department of Physics, University of Washington, Seattle, Washington 98195-1560, USA*

We apply the adiabatic time-dependent density functional theory to magnetic circular dichroism (MCD) spectra using the real-space, real-time computational method. The standard formulas for the MCD response and its $\mathcal{A}$ and $\mathcal{B}$ terms are derived from the observables in the time-dependent wave function. We find real-time method is well suited for calculating the overall spectrum, particularly at higher excitation energies where individual excited states are numerous and overlapping. The MCD sum rules are derived and intepreted in the real-time formalism; we find that they are very useful for normalization purposes and assessing the accuracy of the theory. The method is applied to MCD spectrum of C_{60} using the adiabatic energy functional from the local density approximation. The theory correctly predicts the signs of the $\mathcal{A}$ and $\mathcal{B}$ terms for the lowest allowed excitations. However, the magnitudes of the terms only show qualitative agreement with experiment. © *2011 American Institute of Physics*. [doi:10.1063/1.3575587]

I. INTRODUCTION

Magnetic circular dichroism (MCD) is an important spectroscopic observable useful for characterizing the electronic structure of molecules[1] and condensed matter systems.[2]

To describe MCD spectrum theoretically, several approaches have been developed so far. In early studies,[1] a third-order perturbation theory has been applied in a basis that diagonalizes the zero-field Hamiltonian. This formulation, called the sum-over-states method, requires a considerable computational effort to construct the states and perform the summations.[3,4] A finite field approach has also been employed,[5,6] calculating directly the difference in absorption between lights of left- and right-handed polarization under a finite magnetic field. In this approach, one may avoid construction of the intermediate states. In the last decade, theories based on nonlinear response formalism[7] have been applied extensively to the MCD response.[8–10] In this formalism, response for a perturbation of fixed frequency is solved as a linear algebraic problem, avoiding again a construction of the intermediate states.

We propose here a completely different formalism based on the solution of time-dependent equations of motion and present a formalism for $\mathcal{A}$ and $\mathcal{B}$ terms of the MCD. We find that the formalism is a practical one when applied in the framework of time-dependent density functional theory (TDDFT). In fact, the TDDFT has already been used successfully to calculate MCD in molecules,[4,11–17] using other computational methods. In our formalism, we adopt a finite field approach, calculating the response in time domain with finite electric and magnetic fields. The response coefficients are obtained by numerical differentiation, avoiding the algebraic complexity of nonlinear response theory.

The time domain calculation naturally introduces a finite width effect for discrete transitions. In the response function formalism, similar effect is incorporated by adding a small imaginary part to the frequency.[13,18,19] We may also approximately describe the outgoing boundary condition for electrons emitted to continuum states by putting absorbing potential outside a molecule.[20]

A separate problem in the theory of MCD is the choice of a basis set to construct the electron orbital wave functions. The MCD puts higher demands on the orbital representation to satisfy completeness and gauge invariance than the ordinary dipole response. In the past, an approach employing the London orbital has been developed to ensure gauge invariance of the results in the basis set approach.[5,9,10,21,22] In our treatment, we represent the orbital wave functions on a spatial mesh rather than with atom-centered basis set. The calculated matrix elements are automatically gauge-invariant and one also avoids the inconsistencies that cause sum rules to be violated. The gauge problem has also been discussed in a similar computational approach to ours in relation to calculation of natural circular dichroism.[23]

We mention that the real-time TDDFT has been applied to many observables related to electron dynamics.[24–26] Specific applications include the molecular absorption spectrum in the continuum,[20] hyperpolarizabilities,[27–29] the dielectric function,[30] and chiral dichroism.[23,31] The real-time method has also been applied to phenomena associated with high fields. In the presence of high fields, there is hardly any alternative theory available, at least at the *ab initio* DFT level. Applications include nonlinear electron dynamics in metallic clusters,[32] high harmonic generation,[33] Coulomb

---

a)Electronic mail: bertsch@u.washington.edu.

explosion,[34,35] dielectric breakdown,[36] and coherent phonon generation.[37]

The organization of this article is as follows. In Sec. II we define the time-dependent quantities that are computed and derive the formulas for extracting the observables related to MCD. We also review the sum rules satisfied by the MCD response in Sec. II. In Sec. III we provide some of the numerical details in carrying out the MCD calculations. Following that, in Sec. IV we apply the theory to the C_{60} molecule. Due to its high symmetry, the C_{60} molecule can exhibit both $\mathcal{A}$ and $\mathcal{B}$ terms of MCD. The lowest electronic excitations of this molecule are the $\pi - \pi^*$ character; for the measured transitions we find the correct signs for the calculated $\mathcal{A}$ and $\mathcal{B}$ terms. The theory is also in qualitative agreement with the magnitude of the $\mathcal{B}$ term of the lowest transition. However, the present theory does not reproduce well the other transitions and the magnitude of the $\mathcal{A}$ term.

II. THEORY

A. Definitions for MCD response function

We consider a molecule under a static magnetic field B in γ direction. The electronic Hamiltonian is written as

$$H = H_0 + \mu_B B L_\gamma, \tag{1}$$

where H_0 is the Hamiltonian in the absence of the magnetic field, L_γ is the angular momentum operator, and $\mu_B = e/2mc$ is the Bohr magneton. We take a convention of $e > 0$ and $\hbar = 1$. We denote the ground and excited states under the static magnetic field B as

$$H \Phi_n = E_n \Phi_n. \tag{2}$$

The molecule is excited by the dipole operator $\vec{\mu} = -e \sum \vec{r}_i$ where $\vec{r}_i$ are electron coordinates. We define the circularly polarized dipole operators with the normalization convention $\mu_\pm^{(\gamma)} = (\mu_\alpha \pm i \mu_\beta)/\sqrt{2}$, where $(\alpha\beta\gamma)$ is a cyclic permutation of (xyz).

In MCD, the basic object of study is the difference in dipole absorption strength functions for light of opposite circular polarization in a weak magnetic field. The MCD response may be defined by the strength function

$$R_{\mathrm{MCD}}(E) = \frac{1}{3\mu_B B} \sum_n \sum_\gamma \delta(E - E_{n0})$$
$$\times \{|\langle \Phi_0 | \mu_-^{(\gamma)} | \Phi_n \rangle|^2 - |\langle \Phi_0 | \mu_+^{(\gamma)} | \Phi_n \rangle|^2\}, \tag{3}$$

where E_{n0} is the excitation energy of state n, $E_{n0} = E_n - E_0$. The beam direction coincides with the magnetic field direction along an axis labeled by γ. It is convenient to express the strength function in a Cartesian basis using the antisymmetric tensor $\epsilon_{\alpha\beta\gamma}$,

$$R_{\mathrm{MCD}}(E) = -\frac{1}{3\mu_B B} \sum_{\alpha\beta\gamma} \epsilon_{\alpha\beta\gamma} \sum_n \delta(E - E_{n0})$$
$$\times \mathrm{Im} \left\{ \langle \Phi_0 | \mu_\alpha | \Phi_n \rangle \langle \Phi_n | \mu_\beta | \Phi_0 \rangle \right\}, \tag{4}$$

where the magnetic field is applied to γ direction. We will assume that the ground state is nondegenerate.

To assess the quality of the theory, it is also useful to calculate the ordinary dipole response. We define the dipole response $R_D(E)$ as

$$R_D(E) = \frac{1}{3} \sum_n \sum_\alpha \delta(E - E_{n0}) |\langle \Phi_0 | \mu_\alpha | \Phi_n \rangle|^2, \tag{5}$$

This is related to the oscillator strength distribution by

$$\frac{df}{dE} = \frac{2mE_{n0}}{e^2} R_D(E). \tag{6}$$

Below the ionization threshold, electronic states are discrete. In this energy region, the MCD strength function is often written as

$$R_{\mathrm{MCD}}(E) = \sum_n \left\{ \mathcal{A}_n \left(-\frac{d}{dE} \mathcal{F}_n(E - E_{n0}^{(B=0)}) \right) \right.$$
$$\left. + \mathcal{B}_n \mathcal{F}_n(E - E_{n0}^{(B=0)}) \right\}, \tag{7}$$

where $\mathcal{F}_n(E)$ is the spectral shape of the nth state normalized as $\int \mathcal{F}_n(E) dE = 1$. The zero-field excitation energy is expressed as $E_{n0}^{(B=0)}$. There appear both $\mathcal{A}$ and $\mathcal{B}$ terms for molecules with degeneracy in either ground or excited states, while only $\mathcal{B}$ term appears for molecules without degeneracy in any states. Integrating the MCD response function over an excitation energy around $E_{n0}^{(B=0)}$, we have

$$\mathcal{A}_n = \int_{E_{n0}-\epsilon}^{E_{n0}+\epsilon} dE (E - E_{n0}^{(B=0)}) R_{\mathrm{MCD}}(E), \tag{8}$$

$$\mathcal{B}_n = \int_{E_{n0}-\epsilon}^{E_{n0}+\epsilon} dE R_{\mathrm{MCD}}(E), \tag{9}$$

where ϵ is a small energy interval. These terms may be expressed perturbatively in terms of the energy and the wave functions in the absence of the magnetic field. In the following two Eqs. (10) and (11) energy eigenvalues and wave functions refer to those in the absence of the magnetic field.

For $\mathcal{A}$, we have

$$\mathcal{A}_n = -\frac{1}{3} \sum_{\alpha\beta\gamma} \epsilon_{\alpha\beta\gamma} \sum_t \left\{ (L_\gamma)_{nt,nt} - (L_\gamma)_{0,0} \right\}$$
$$\times \mathrm{Im} \langle \Phi_0 | \mu_\alpha^{(\gamma)} | \Phi_{nt} \rangle \langle \Phi_{nt} | \mu_\beta^{(\gamma)} | \Phi_0 \rangle, \tag{10}$$

where t distinguishes degenerate excited states in a basis that diagonalizes L_γ. For $\mathcal{B}$, we have

$$\mathcal{B}_n = \frac{2}{3} \mathrm{Im} \sum_{\alpha\beta\gamma} \epsilon_{\alpha\beta\gamma}$$
$$\times \sum_m \left\{ \frac{1}{E_{m0}} \langle \Phi_m | L_\gamma | \Phi_0 \rangle \langle \Phi_0 | \mu_\alpha | \Phi_n \rangle \langle \Phi_n | \mu_\beta | \Phi_m \rangle \right.$$
$$\left. + \frac{1}{E_{mn}} \langle \Phi_n | L_\gamma | \Phi_m \rangle \langle \Phi_0 | \mu_\alpha | \Phi_n \rangle \langle \Phi_m | \mu_\beta | \Phi_0 \rangle \right\}. \tag{11}$$

Similarly, we define the ordinary dipole strength as

$$\mathcal{D}_n = \int_{E_{n0}-\epsilon}^{E_{n0}+\epsilon} dE R_D(E) = \frac{1}{3} \sum_\alpha |\langle \Phi_0 | \mu_\alpha | \Phi_n \rangle|^2. \tag{12}$$

It is related to the oscillator strength f_n as $f_n = 2m E_{n0} \mathcal{D}_n / e^2$.

Finally, with our definition of the MCD response, the $\mathcal{B}$ coefficient is related to the ratio of the MCD extinction coefficient $\Delta \epsilon$ to the ordinary extinction coefficient ϵ by the formula

$$\frac{\Delta \epsilon}{\epsilon} = \frac{2m \mu_B B E_{n0} \mathcal{B}_n}{e^2 f_n}. \tag{13}$$

B. Real-time formulation

The response associated with any pair of operators, $\mathcal{O}_1$ and $\mathcal{O}_2$, may be calculated in the real-time domain starting from the ground state wave function Φ_0. One first applies an impulsive perturbation $\lambda \mathcal{O}_1$ to obtain an initial wave function $\Psi(t = 0_+)$. This is then evolved in time with the exponentiated Hamiltonian operator,

$$\Psi(t) = e^{-iHt} e^{i\lambda \mathcal{O}_1} \Phi_0. \tag{14}$$

The real-time response $S_{21}(t)$ is given by the expectation value of the operator $\mathcal{O}_2$ in that state,

$$S_{21}(t) = \langle \Psi(t) | \mathcal{O}_2 | \Psi(t) \rangle. \tag{15}$$

The linear response is evaluated by treating λ as a small parameter and taking the derivative $dS_{21}(t)/d\lambda$ at $\lambda = 0$. Depending on the operators $\mathcal{O}_1$ and $\mathcal{O}_2$, the strength function R_{21} is obtained as the imaginary or real part of the Fourier transform of linear response $dS_{21}(t)/d\lambda|_{\lambda=0}$ on the time interval $[0, +\infty]$.

This general formulation of the linear response applies to the MCD strength function Eq. (4) taking the operators to be $\mathcal{O}_1 = \mu_\beta$ and $\mathcal{O}_2 = \mu_\alpha$. The wave function is set up at $t = 0$ as $\Psi_{k\beta}(t = 0_+) = e^{ik\mu_\beta} \Phi_0$ and the real-time response $S_{\alpha\beta}^{(\gamma)}(t)$ is given by

$$S_{\alpha\beta}^{(\gamma)}(t) = \langle \Psi_{k\beta}(t) | \mu_\alpha | \Psi_{k\beta}(t) \rangle, \tag{16}$$

where (γ) in $S_{\alpha\beta}^{(\gamma)}$ is included to remember that a static magnetic field is applied to γ direction throughout the time evolution. Expanding the perturbing operator $e^{ik\mu_\beta}$ in powers of k, we have

$$
\begin{aligned}
S_{\alpha\beta}^{(\gamma)}(t) = ik & \left\{ \langle \Phi_0 | \mu_\alpha e^{-i(H-E_0)t} \mu_\beta | \Phi_0 \rangle \right. \\
& \left. - \langle \Phi_0 | \mu_\beta e^{i(H-E_0)t} \mu_\alpha | \Phi_0 \rangle \right\}, \\
= ik & \sum_n \langle \Phi_0 | \mu_\alpha | \Phi_n \rangle \langle \Phi_n | \mu_\beta | \Phi_0 \rangle e^{-iE_{n0}t} \\
& - ik \sum_n \langle \Phi_0 | \mu_\beta | \Phi_n \rangle \langle \Phi_n | \mu_\alpha | \Phi_0 \rangle e^{iE_{n0}t}. \tag{17}
\end{aligned}
$$

In the last formula, we have expressed the time-evolution operator in terms of the energy eigenstates of the system. We next separate out the time-even and time-odd parts of the response, writing it as

$$
\begin{aligned}
S_{\alpha\beta}^{(\gamma)}(t) = & -2k \sum_n \text{Im} \left\{ \langle \Phi_0 | \mu_\alpha | \Phi_n \rangle \langle \Phi_n | \mu_\beta | \Phi_0 \rangle \right\} \cos E_{n0}t \\
& + 2k \sum_n \text{Re} \left\{ \langle \Phi_0 | \mu_\alpha | \Phi_n \rangle \langle \Phi_n | \mu_\beta | \Phi_0 \rangle \right\} \sin E_{n0}t. \tag{18}
\end{aligned}
$$

The combination $S_{\alpha\beta}^{(\gamma)} - S_{\beta\alpha}^{(\gamma)} = -4k \sum_n \text{Im}\{\langle \Phi_0 | \mu_\alpha | \Phi_n \rangle \langle \Phi_n | \mu_\beta | \Phi_0 \rangle\} \cos E_{n0}t$ isolates the first term with the cosine dependence on time. We obtain an expression proportional to the MCD response by taking its cosine Fourier transform,

$$
\begin{aligned}
& -\frac{1}{2\pi k} \int_0^\infty dt \cos Et \left\{ S_{\alpha\beta}^{(\gamma)} - S_{\beta\alpha}^{(\gamma)} \right\} \\
& = \sum_n \text{Im} \left\{ \langle \Phi_0 | \mu_\alpha | \Phi_n \rangle \langle \Phi_n | \mu_\beta | \Phi_0 \rangle \right\} \delta(E - E_{n0}). \tag{19}
\end{aligned}
$$

The MCD strength function with the proper prefactor is given by the integral over the real-time response as

$$R_{\text{MCD}}(E) = \frac{1}{6\pi \mu_B B k} \sum_{\alpha\beta\gamma} \epsilon_{\alpha\beta\gamma} \int_0^\infty dt \cos Et \left\{ S_{\alpha\beta}^{(\gamma)} - S_{\beta\alpha}^{(\gamma)} \right\}. \tag{20}$$

For the molecules we treat here, we can choose coordinate systems such that the off-diagonal response is antisymmetric, $S_{\alpha\beta}^{(\gamma)}(t) = -S_{\beta\alpha}^{(\gamma)}(t)$. Then the second term in Eq. (18) is identically zero and Eq. (20) reduces to

$$R_{\text{MCD}}(E) = \frac{2}{3\pi \mu_B B k} \int_0^\infty dt \cos Et \left\{ S_{xy}^{(z)}(t) + S_{yz}^{(x)}(t) + S_{zx}^{(y)}(t) \right\}. \tag{21}$$

This is our main result that will be applied to calculate the MCD.

For most if not all MCD spectra, the sign of $R_{\text{MCD}}(E)$ on the infrared side of the lowest optical excitation is negative. We shall call this the "normal" sign.

The ordinary dipole response $R_D(E)$ may also be computed in the formalism as Fourier sine transform,

$$R_D(E) = \frac{1}{3\pi k} \sum_\alpha \int_0^\infty dt \sin Et \, S_{\alpha\alpha}^{(\gamma)}(t). \tag{22}$$

Note that this can easily be evaluated at the same time as $R_{\text{MCD}}(E)$ because the same time-dependent wave function is used in both.

C. Sum rules

The real-time formalism is very convenient for evaluating and verifying energy-weighted sum rules. In particular, the MCD response satisfies a quadratic sum rule that depends only on the magnetic field strength and the number of electrons.[38] The connection to the time-dependent response may be easily derived by expanding $S_{\alpha\beta}^{(\gamma)}$ as a power series in time t,

$$S_{\alpha\beta}^{(\gamma)}(t) \simeq s_0 + s_2 t^2 + \cdots. \tag{23}$$

Only even powers of t are present in the series expansion, due to the suppression of the second term in Eq. (18). The coefficients s_0 and s_2 can be readily expressed as commutators of the μ operators and the Hamiltonian and evaluated analytically. One finds

$$
\begin{aligned}
s_0 & = -2k \text{Im} \sum_n \left\{ \langle \Phi_0 | \mu_\alpha | \Phi_n \rangle \langle \Phi_n | \mu_\beta | \Phi_0 \rangle \right\} \\
& = ik \langle \Phi_0 | [\mu_\alpha, \mu_\beta] | \Phi_0 \rangle = 0, \tag{24}
\end{aligned}
$$

and

$$s_2 = k\mathrm{Im} \sum_n \left\{ \langle \Phi_0 | \mu_\alpha | \Phi_n \rangle \langle \Phi_n | \mu_\beta | \Phi_0 \rangle \right\} E_{n0}^2$$

$$= -\frac{ik}{2} \langle \Phi_0 | [\mu_\alpha, [H, [H, \mu_\beta]]] | \Phi_0 \rangle = \pm \frac{e^3 Bk}{2m^2 c} N_e, \quad (25)$$

where N_e is the number of electrons and the sign reflects the order of $(\alpha\beta\gamma)$. These formulas can be expressed as integrals over the MCD strength function:

$$I_0 = \int_0^\infty dE\, R_{\mathrm{MCD}}(E) = 0, \quad (26)$$

$$I_2 = \int_0^\infty dE\, E^2 R_{\mathrm{MCD}}(E) = \frac{2e^2}{m} N_e. \quad (27)$$

The I_2 sum rule has a simple physical interpretation. Consider the real-time response associated with $S_{xy}^{(z)}$. The impulsive exciting potential $eky\,\delta(t)$ gives the electrons an average momentum equal to $-ek\hat{y}$, the integral of the force over time. The corresponding velocity, $\vec{v} = -ek\hat{y}/m$, is subject to a magnetic force $-e\vec{v} \times \vec{B}/c$ which is in the x direction for our geometry. The corresponding acceleration is $a = e^2 Bk\hat{x}/m^2 c$. Thus the x-component of the dipole moment increases quadratically with time according to the acceleration formula

$$\langle -ex(t) \rangle = \frac{1}{2} at^2 = \frac{N_e e^3 Bk}{2m^2 c} t^2, \quad (28)$$

in agreement with Eqs. (23) and (25).

In the results of the calculations given below, we will also show the performance of the theory with respect to the f-sum rule. In terms of the response $R_D(E)$, we define the quantity

$$f_E = 2m \int_0^E dE'\, E'\, R_D(E'). \quad (29)$$

The sum rule is given by

$$f_{+\infty} = N_e, \quad (30)$$

where N_e is the number of electrons. The associated short-time behavior of the real-time response is linear in t and given by

$$\langle \Psi_{k\alpha}(t) | \mu_\alpha | \Psi_{k\alpha}(t) \rangle \approx \frac{e^2 k}{m} N_e t. \quad (31)$$

D. Time-dependent density functional theory

The basic variables in Kohn–Sham density functional theory are the orbitals $\phi_i(\vec{r})$, which are varied to minimize an energy expression E_{KS} that contains the quantum kinetic operator and terms depending on the density $n(\vec{r}) = \sum_i |\phi_i(\vec{r})|^2$. The formal variation of the E_{KS} energy expression with respect to an orbital gives the Kohn–Sham operator H_{KS}. In the time-dependent extension of DFT with the adiabatic approximation, the operator H_{KS} is also used in the equation of motion for the orbitals. For linear order in the magnetic field strength B, the time-dependent orbitals satisfy the equation

$$[H_{KS} + \mu_B \vec{L} \cdot \vec{B}] \psi_i(t) = i \frac{\partial}{\partial t} \psi_i(t). \quad (32)$$

This equation is solved for $\psi_i(t)$ with initial condition $\psi_i(t = 0_+) = e^{ik\mu_\beta} \phi_i(\vec{r})$, where ϕ_i are the ground-state Kohn–Sham orbitals. The time-dependent response is calculated as

$$S_{\alpha\beta}^{(\gamma)}(t) = \sum_i \langle \psi_i(t) | \mu_\alpha | \psi_i(t) \rangle. \quad (33)$$

For the calculations described below, we treat only the valence electrons dynamically and ignore any spin dependence. The effects of core electrons are treated by using Troullier–Martins pseudopotentials for the electron–ion interaction.[39] We use the usual local-density approximation (LDA) functional[40] for the exchange-correlation interaction as in the previous work.[41]

III. COMPUTATIONAL ASPECTS

The implementation of our real-time TDDFT is described in detail in Ref. 25. An important difference from other TDDFT codes is the orbital representation in three-dimensional Cartesian mesh. This has the computational benefit that the Kohn–Sham operator is given by a sparse matrix. The representation is also convenient for treating extended wave functions such as Rydberg states or continuum states. It has the disadvantage, however, that it does not permit all-electron calculations with practical mesh sizes. For checking our code, we found it helpful to calculate the observables with the Troullier–Martins pseudopotential replaced by an anisotropic harmonic oscillator potential. All the observables in this model have analytic expressions that can be compared with the calculated numerical quantitites. See the Appendix for details.

In our implementation of the mesh representation, the momentum operator p is computed by the 8-point difference function, which is consistent with our treatment of the kinetic operator $p^2/2m$ as a sum of 9-point difference functions along the three Cartesian axes. The main numerical parameters in the calculation are the mesh spacing Δx, the size of the spatial domain on which the orbital wave functions are defined, the time step Δt, and the total integration time T. We find that adequate precision for our purposes is obtained with parameter values $\Delta x = 0.5$ and $\Delta t = 0.03$ in atomic units. The spatial dimensions needed for the orbital wave functions depend on the desired accuracy in the continuum region. The continuum strength functions are smooth only if the spatial domain is large and absorbing boundary conditions are applied at the edges. Typically, we take a cubical box of 160^3 mesh points for the calculations. For small molecules, a much smaller domain is adequate if the details of the response in the continuum are not needed.

Although the TDDFT is fundamentally nonperturbative, the quantities we calculate are in fact the perturbative limits with respect to the strengths of the applied magnetic and electric fields. We thus choose strengths that are small enough for the linear response formula to apply, but large enough to avoid numerical round-off errors. For the perturbing electric field, we take $k = 0.001$. For the magnetic field, the calculations reported below were carried out with a magnetic field given by $\mu_B B = 0.0005$ a.u. The intensity of this magnetic field is

0.137 a.u. For comparison, a field strength of one Tesla has the value 5.81×10^{-4} in atomic units.

The integration time T required to calculate the response depends on the desired energy resolution. We multiply the integrands in the Fourier transforms Eqs. (20) and (22) by the filter function $1 - 3(t/T)^2 + 2(t/T)^3$ to smooth out spurious oscillations from the upper time cutoff. The resulting peaks associated with sharp states have a width Γ (full width at half maximum) given approximately by $\Gamma \approx 6/T$. Most of our results were calculated by integrating $N_t = 60000$ time steps, giving $\Gamma \approx 6/(N_t \Delta t) \sim 0.0033$ a.u. $= 0.1$ eV.

IV. APPLICATION TO C_{60}

The C_{60} molecule offers a good test of the methodology to demonstrate the feasibilty of using the real-time method as applied to fairly large molecules. Due to the high symmetry of C_{60}, all optically allowed transitions are threefold degenerate and there will be both $\mathcal{A}$ and $\mathcal{B}$ terms in the MCD spectrum. There are 5–6 excitations in the calculated spectrum up to 6 eV, all of which are $\pi - \pi^*$ character. It has been found that the experimental oscillator strength[42,43] accords well with the theory[41] based on the *ab initio* adiabatic local density approximation.

Our calculation here is very similar to that carried out in Ref. 41 for the oscillator strength function. The integration time in the present calculation is somewhat longer, 60,000 time steps with $\Delta t = 0.03$ a.u. Before examining the MCD response, we recall the results for the ordinary dipole response, as calculated in the real-time method. Figure 1 shows the $S_{zz}(t)$ real-time response over the interval $[0, T] = [0, 25]$ fs with the upper panel showing an expanded view of the first 0.275 fs time interval.

The short-time behavior expected from Eq. (31) is shown by the straight dotted line in the upper panel. One may see that the initial response does indeed follow Eq. (31) very well. After the initial rise in the first 0.1 fs the dipole moment oscillates with a period of order of 1 fs corresponds to the strong transitions in the energy interval 7–15 eV. Note that the oscillation is essentially undamped. This is a consequence of the sharpness of the bound excitations that would produce a δ-function response if the Fourier transform could be done exactly. The numerical Fourier transform was carried out to final time $t = 1800$ a.u. $= 43.5$ fs with the results for the low-frequency part of $R_D(E)$ shown in the upper panel of Fig. 2. There are four transitions in the spectral region 0–6 eV, at excitation energies of 3.5, 4.3, 5.3, and 5.9 eV. The numerical FWHM widths are about 0.1 eV, as expected from the integration time. The important information besides the transition energy is total strength in the individual peaks. This can be extracted from the graph of the integrated strength f_E defined in Eq. (29).

The jumps at low energies give the f strengths of the discrete transitions. The total integrated strength is $f = 233$, rather close to the sum rule number $f = 240$ for $N_e = 240$ valence electrons treated dynamically in the TDDFT. We note that the sum rule is not expected to be satisfied exactly for our energy functional, because of nonlocality in the Troullier–Martins pseudopotential.
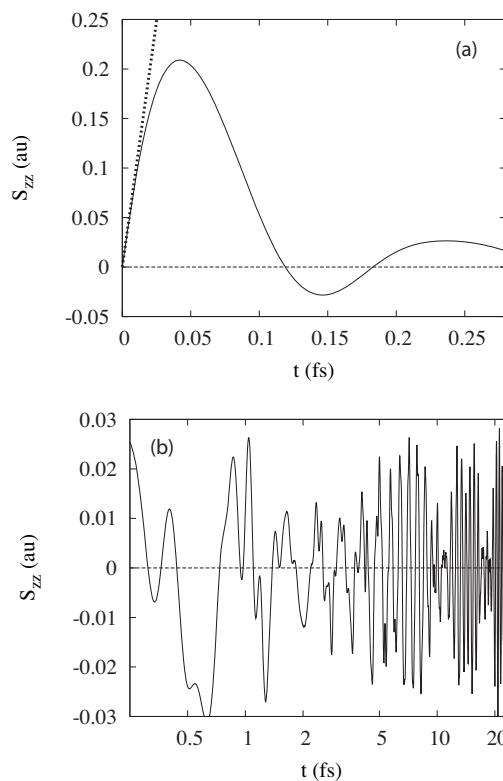

FIG. 1. Real-time dipole response $S_{zz}(t) = \langle \Psi_{kz}(t)|\mu_z|\Psi_{kz}(t)\rangle$ for C_{60}. The upper panel shows the time interval $t = 0 - 0.275$ fs with a linear time scale. The sloping line shows the expected short-time behavior according to Eq. (31). The lower panel shows the time interval $t = 0.25 - 25.0$ fs on a logarithmic time scale.
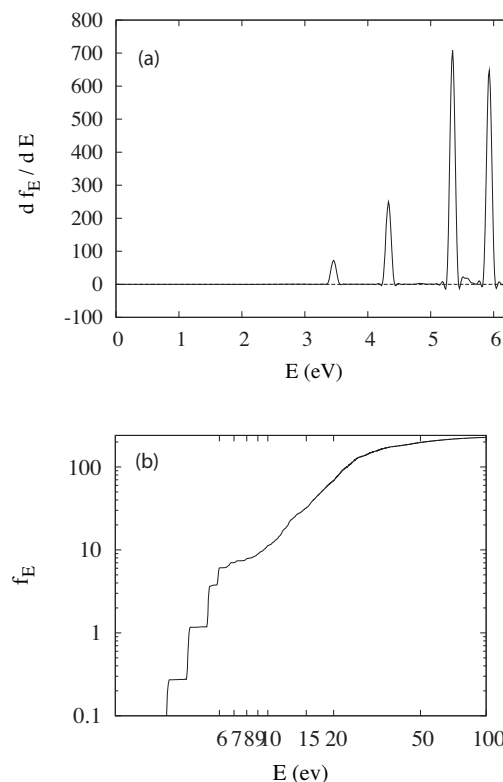

FIG. 2. Dipole response for C_{60}. The differential oscillator strength df/dE [Eq. (6)] up to 6 eV is shown in the upper panel. The lower panel shows the integrated oscillator strength function, f_E, Eq. (29).
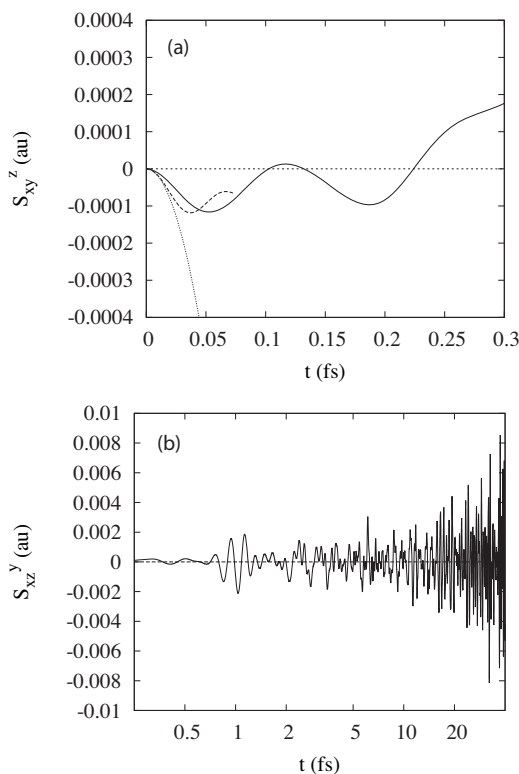
FIG. 3. MCD real-time response $S_{xy}^{(z)}$ in C_{60}. The solid line in upper panel shows the evolution for short times, $0 < t < 0.3$ fs. The dotted curve is the expected dependence from Eq. (28). The long-dashed curve shows the response in the time range $0 < t < 0.07$ fs with the nonlocality in the pseudopotential turned off. The lower panel shows the response in the longer time interval $0.25 < t < 40$ fs on a logarithmic time scale and a magnified ordinate scale.
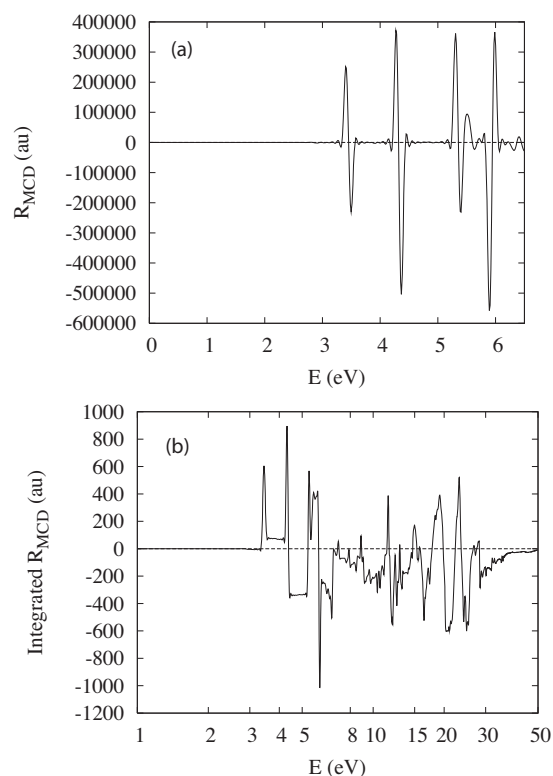

FIG. 4. MCD response $R_{MCD}(E)$ in C_{60}. Upper panel shows the strength function Eq. (4). The corresponding integrated strength function is shown in the lower panel.

We now take up the MCD response. The upper panel of Fig. 3 shows the calculated MCD real-time response $S_{xy}^{(z)}(t)$ over the time interval $0 < t < 0.3$ fs. The dashed curve in the upper panel shows the predicted short-time dependence according to Eq. (28). The computed time dependence starts out quadratic as expected, but the coefficient of t^2 is lower by 40% than expected from Eq. (28). To confirm that the nonlocality of the pseudopotential is responsible for the disagreement, we have recomputed the response for short times with nonlocality of the pseudopotentials turned off, shown as the long-dashed line in Fig. 3. This agrees closely with the expected short-time behavior. We do not have any explanation why the sum rule violation is much stronger for the MCD strength than for the ordinary dipole strength.

The MCD response going to long times is shown on the lower panel of Fig. 3. It is interesting to note that the amplitude of oscillation increases with time. This behavior is in contrast to the ordinary dipole response, which has a maximum excursion in the first oscillation. The reason for the increase in amplitude is the presence of the $\mathcal{A}$ terms which give a real-time response that cancels at short times and only becomes visible at later times.

Taking the Fourier cosine transform of the real-time response using Eq. (20) we find the MCD spectrum shown in Fig. 4 upper panel. The $\mathcal{A}$-type character of the $\pi - \pi^*$ transitions is clearly seen in the shape of curves, each with a strong

alternation of sign over the width of the peaks in the dipole response function. (Again, there is no physical significance to the calculated widths since they depend on the integration limit in the Fourier transform.) It is interesting to see that the sign of $\mathcal{A}$ coefficients can vary from state to state. The excitation at 5.9 eV has the normal sign, namely negative on the low-frequency side, but the three lower excitations have the opposite sign. The four transitions in the figure also have a significant $\mathcal{B}$-type MCD response, visible by unequal positive- and negative-going peaks on the two sides of the transition. The $\mathcal{B}$-type response may be seen more clearly in the graph of the integrated MCD response, $\int^E dE' R_{MCD}(E')$, shown on the lower panel of Fig. 4. The $\mathcal{B}_n$ coefficients can be read off from the step increases going across each transition, cf. Eq. (9). The values are reported in Table I divided by the theoretical dipoles strengths $\mathcal{D}_n$ [Eq. (12)]. This is to facilitate

TABLE I. MCD response of the lowest four $^1T_{1u}$ states in C_{60}. The experimental data is from Ref. 44. Our calculations are given in the columns labeled TDDFT. The effective orbital g-factor is defined in Eq. (34).

Energy (eV)		$\mathcal{B}_n/\mathcal{D}_n$		g		
Exp.	TDDFT	Exp.	TDDFT	Exp.	TDDFT	Ref. 45
3.8	3.5	100	64	-0.3 ± 0.05	-0.97	-1.0
4.9	4.3	-700	-146	-0.55 ± 0.15	-0.58	-0.75
6.0	5.3		66		-0.20	$+0.12$
	5.9		-120		$+0.35$	

comparison to the experimental values,[44] which are given in this form. We see that the signs of $\mathcal{B}_n$ for the lowest two states agree. This is far from trivial. Also, the calculated magnitude of the lower one is within a factor of 2 of experiment. This is a poorer agreement than is typical for the calculation of oscillator strength f_n in TDDFT, but perhaps this should not be unexpected due to the difficulties uncovered by the unexpected short-time behavior. Also, we know that there is considerable screening of the valence-electron transition moments, amplifying the relative errors of the screened observables. The $\mathcal{B}_n$ of the second state has a much larger discrepancy. Until that is understood, one cannot use the TDDFT as a predictive tool for large molecules.

For a overall view of the MCD response, the lower panel of Fig. 4 shows the integrated MCD response up to 50 eV. The integrated response is predominantly negative, as to be expected with the negative-going initial evolution. One sees that the total goes to zero at the upper energy, showing that the I_0 sum rule [Eq. (26)] is nearly satisfied. Finally, the E^2 sum rule, Eq. (27) has a value $I_2 = 258$, almost a factor of 2 smaller than the nominal value of $2N_e = 480$. We have already seen this effect of the nonlocality in the short-time response.

We next turn to the $\mathcal{A}$-type response, arising from the energy splitting between members of $^1T_{1u}$ multiplets as in the Zeeman splitting. A convenient way to express the splitting is as the effective g-factor for the transition[1][Eq. (52)],

$$g = \frac{\Delta E}{\mu_B B}. \tag{34}$$

This is related to $\mathcal{A}_n$ by

$$g = \frac{\mathcal{A}_n}{2\mathcal{D}_n}. \tag{35}$$

We extract the $\mathcal{A}_n$ coefficients by Eq. (8) from $R_{MCD}(E)$. We may also extract the energy shift ΔE from the zero-field value using the formula

$$\Delta E = -\mu_B B \frac{\int_{E_{n0}-\epsilon}^{E_{no}} dE\, R_{MCD}(E) - \int_{E_{n0}}^{E_{no+\epsilon}} dE\, R_{MCD}(E)}{4R_D(E_{n0})}. \tag{36}$$

The extracted g-factors are shown in Table I along with the measured values[44] and results of a model calculation.[45]

As with the $\mathcal{B}_n$ values, we see agreement on sign for the two measured transitions. However, only the upper transition has a magnitude consistent with experiment.

V. CONCLUDING REMARKS

We have shown that from a computational point of view, the real-time method is a practical approach to calculate the MCD response in TDDFT. We here mention advantages and disadvantages of the real-time approach comparing it with other approaches. The real-time approach resembles, to some extent, to response function approaches,[8,15,16,18] since they are related to each other by Fourier transformation. In the response function approaches, linear algebraic equation needs to be solved at each frequency, while the entire response in the energy region of valence-electron excitations is obtained

from a single calculation in the real-time calculation. Therefore, the real-time approach will be suitable to get information of a whole spectral region, while the response function approach will be appropriate if one is interested in the response at a limited frequency region.

Another advantage of the present real-time approach is its simplicity in the coding. This comes from the fact that we adopt a finite field approach, applying a static magnetic field of finite magnitude in the calculation. The additional coding to the ground state calculation is the time evolution of the Kohn–Sham orbitals, which may be achieved with a rather small amount of coding.

The principal drawback of the present approach may be a rather high computational cost for small systems compared with methods employing atomic basis sets. However, the computational cost of the present approach scales rather slow for the system size. The ground state calculation scales $O(N^3)$ where N denotes the system size, while the real-time calculation scales $O(N^2)$ for a fixed number of time steps. We may also compute efficiently in parallel machines dividing spatial grid points into different processors.[35]

In the real-time approach, sum rules may be used, at least as a theoretical tool, to understand the limitations with respect to the omission of core electrons from the dynamics. It would be exceedingly challenging to ensure that the sum rules, Eqs. (26) and (27) are obeyed in formalisms that employs a basis set. The violation of the sum rule, Eq. (27) in the valence particle space raises an issue that needs to be addressed in future work. In Ref. 46 it was found that the violation of the dipole response in TDDFT is largely justified. The dynamic contribution of the core electrons shifts oscillator strength down into the spectral region of valence electrons, and this accounts physically for the increase of the sum rule, calculated only with valence electrons employing the nonlocal pseudopotential in the space of valence-electron excitations. Whether there is a related mechanism to the decrease in the I_2, sum rule remains to be seen. Also, the pseudopotential should in principle be corrected for the gauge field associated with the magnetism, but that was not done here. It should be mentioned that these questions will also arise on calculations using the projected augmented wave (PAW) method,[47] since this also makes the Kohn–Sham operator nonlocal.

It was also a surprise to us to find that the MCD response may have an abnormal sign. This goes against the picture of an electron being excited to a higher band of orbitals and there undergoing circular motion in the sense given by the external magnetic field. It might be that strong screening destroys the simple connection to the expected classical oscillation picture. This raises another question for future work to investigate in a general way the effects of screening on the MCD.

Finally, we have not discussed here the sensitivity to specific density functionals. Although not reported, we have also carried out the C_{60} calculations with the LB94 functional.[48] This gave very similar results except for Rydberg transitions, which are considerably shifted in energy, depending on the functional. Since the observables in MCD depend on currents, it might also be interesting to investigate the generalized TDDFT including current–current interactions.

APPENDIX: ANISOTROPIC HARMONIC OSCILLATOR MODEL

In this Appendix we apply the real-time theory to a simple Hamiltonian, a spinless electron in an anisotropic harmonic oscillator potential. The model is completely solvable making it useful in checking the coding and formulas for the TDDFT in a magnetic field.

The Hamiltonian H_0 in Eq. (1) is taken as

$$H_0 = \frac{p^2}{2m} + \frac{1}{2}\sum_\alpha^3 m\omega_\alpha^2 r_\alpha^2. \tag{A1}$$

We label the eigenstates of H_0 by the number of excitation quanta along each coordinate axis, $|n_x n_y n_z\rangle$, and we set $m = e = \hbar = 1$ in the equations below. We take the oscillator frequencies ω_α to be nondegenerate, so the MCD response will only have $\mathcal{B}$-type contributions. We first need the eigenstates in the presence of the magnetic field, expanded to first order in the field strength. Taking the magnetic field in the z-direction, the relevant perturbed orbitals are

$$|000, B_z\rangle = |000\rangle - i s_0 |110\rangle, \tag{A2}$$

$$|100, B_z\rangle = |100\rangle - i s_1 |010\rangle,$$

$$|010, B_z\rangle = |010\rangle - i s_1 |100\rangle,$$

where

$$s_{0,1} = \frac{\mu_B B_z}{2}\frac{\omega_y \mp \omega_x}{(\omega_y \pm \omega_x)(\omega_x \omega_y)^{1/2}}. \tag{A3}$$

The perturbed energies of the orbitals are not needed because that perturbation is second order in B_z.

To get the real-time response $S_{xy}^{(z)}$, we multiply the ground state wave function by the field $e^{ik\mu_y}$ and expand over the eigenstates, to first order in k. The required matrix elements of the dipole operator between ground and excited states are

$$\langle 100, B_z | \mu_x | 000, B_z \rangle = (2\omega_x)^{-1/2}, \tag{A4}$$

$$\langle 010, B_z | \mu_y | 000, B_z \rangle = (2\omega_y)^{-1/2},$$

$$\langle 010, B_z | \mu_x | 000, B_z \rangle = -i\mu_B B_z (2\omega_y)^{1/2}/(\omega_x^2 - \omega_y^2),$$

$$\langle 100, B_z | \mu_y | 000, B_z \rangle = -i\mu_B B_z (2\omega_x)^{1/2}/(\omega_x^2 - \omega_y^2).$$

The initial perturbed wave function is

$$|\Psi_{ky}(t=0)\rangle = |000, B_z\rangle + i\frac{k}{(2\omega_y)^{1/2}}|010, B_z\rangle$$

$$+ \mu_B B_z k \frac{(2\omega_x)^{1/2}}{(\omega_x^2 - \omega_y^2)}|100, B_z\rangle. \tag{A5}$$

The time dependence is put in by multiplying the excited states by $e^{-i\omega_\alpha t}$. The expectation value of μ_x may then be evaluated as a function of time. The result after some simplification is

$$S_{xy}^{(z)} = \frac{2k\mu_B B_z}{\omega_x^2 - \omega_y^2}(\cos\omega_x t - \cos\omega_y t). \tag{A6}$$

The short-time response given by Eq. (27) may be verified by making a power series expansion of the cosine functions in Eq. (A6). Finally, the evaluation of R_{MCD} by Eq. (20) may be verified by carrying out the cosine Fourier transform, $(2/\pi)\int_0^\infty dt \cos\omega t \cos\omega_0 t = \delta(\omega - \omega_0)$. Putting in all three magnetic moment directions, the result is

$$R_{\mathrm{MCD}} = -\frac{1}{3}\frac{1}{\mu_B B}\sum_{\beta \neq \alpha}\delta(E - \omega_\alpha)\frac{2}{\omega_\alpha^2 - \omega_\beta^2}. \tag{A7}$$

It may be easily verified that R_{MCD} satisfies the two sum rules, Eqs. (25) and (26).

[1] P. J. Stephens, Adv. Chem Phys. **35**, 197 (1976).
[2] H. Wende, Rep. Prog. Phys. **67**, 2105 (2004).
[3] Y. Honda, M. Hada, M. Ehara, H. Nakatsuji, and J. Michl, J. Chem. Phys. **123**, 164113 (2005).
[4] M. Seth, J. Autschbach, and T. Ziegler, J. Chem. Theory Comput. **3**, 434 (2007).
[5] L. Seamans and J. Linderberg, Mol. Phys. **24**, 1393 (1972).
[6] D. Ganyushin and F. Neese, J. Chem. Phys. **128**, 114117 (2008).
[7] J. Olsen and P. Jørgensen, J. Chem. Phys. **82**, 3235 (1985).
[8] S. Coriani, P. Jørgensen, A. Rizzo, K. Ruud, and J. Olsen, Chem. Phys. Lett. **300**, 61 (1999).
[9] S. Coriani, C. Hättig, P. Jørgensen, and T. Helgaker, J. Chem. Phys. **113**, 3561 (2000).
[10] T. Kjærgaard, B. Jansik, P. Jørgensen, S. Coriani, and J. Michl, J. Phys. Chem. A **111**, 11278 (2007).
[11] M. Seth, T. Ziegler, A. Banerjee, J. Autschbach, S. J. A. van Gisbergen, and E. J. Baerends, J. Chem. Phys. **120**, 10942 (2004).
[12] M. Seth and T. Ziegler, J. Chem. Phys. **127**, 134108 (2007).
[13] M. Krykunov, M. Seth, T. Ziegler, and J. Autschbach, J. Chem. Phys. **127**, 244102 (2007).
[14] H. Solheim, L. Frediani, K. Ruud, and S. Coriani, Theor. Chem. Acc. **119**, 231 (2008).
[15] M. Seth, M. Krykunov, T. Ziegler, J. Autschbach, and A. Banerjee, J. Chem. Phys. **128**, 144105 (2008).
[16] M. Seth, M. Krykunov, T. Ziegler, J. Autschbach, J. Chem. Phys. **128**, 234102 (2008).
[17] M. Seth, T. Ziegler, and J. Autschbach, J. Chem. Phys. **129**, 104105 (2008).
[18] H. Solheim, K. Ruud, S. Coriani, and P. Norman, J. Chem. Phys. **128**, 094103 (2008).
[19] K. Kristensen, J. Kauczor, T. Kjærgaard, and P. Jørgensen, J. Chem. Phys. **131**, 044112 (2009).
[20] T. Nakatsukasa and K. Yabana, J. Chem. Phys. **114**, 2550 (2001).
[21] M. Krykunov, A. Banerjee, T. Ziegler, and J. Autschbach, J. Chem. Phys. **122**, 074105 (2005).
[22] T. Kjærgaard, P. Jørgensen, A. J. Thorvaldsen, P. Sałek, and S. Coriani, J. Chem. Theor. Comput. **5**, 1997 (2009).
[23] D. Varsano, L. A. Espinosa-Leal, X. Andrade, M. A. L. Marques, R. di Felice, and A. Rubio, Phys. Chem. Chem. Phys. **11**, 4481 (2009).
[24] K. Yabana and G. F. Bertsch, Phys. Rev. B **54**, 4484 (1996).
[25] K. Yabana, T. Nakatsukasa, J.-I. Iwata, and G. F. Bertsch, Phys. Status Solidi B **243**, 1121 (2006).
[26] A. Castro, H. Appel, M. Oliveira, C. A. Rozzi, X. Andrade, F. Lorenzen, M. A. L. Marques, E. K. U. Gross, A. Rubio, Phys. Status Solidi B **243**, 2465 (2006).
[27] J.-I. Iwata, K. Yabana, and G. F. Bertsch, J. Comput. Meth. Sci. Eng. **4**, 461 (2004).
[28] Y. Takimoto, F. G. Vila, and J. J. Rehr, J. Chem. Phys. **127**, 154114 (2007).
[29] X. Andrade, S. Botti, M. A. L. Marques, A. Rubio, J. Chem. Phys. **126**, 184106 (2007).

[30] G. F. Bertsch, J.-I. Iwata, A. Rubio, and K. Yabana, Phys. Rev. B **62**, 7998 (2000).

[31] K. Yabana and G. F. Bertsch, Phys. Rev. A **60**, 1271 (1999).

[32] F. Calvayrac, P.-G. Reinhard, E. Suraud, and C. A. Ullrich, Phys. Rep. **337**, 493 (2000).

[33] K. Nobusada and K. Yabana, Phys. Rev. A **70**, 043411 (2004).

[34] A. Castro, M. A. L. Marques, J. A. Alonso, G. F. Bertsch, A. Rubio, Eur. Phys. J. D **28**, 211 (2004).

[35] Y. Kawashita, T. Nakatsukasa, and K. Yabana, J. Phys. Condens. Matter **21**, 064222 (2009).

[36] T. Otobe, M. Yamagiwa, J.-I. Iwata, K. Yabana, T. Nakatsukasa, G. F. Bert, Phys. Rev. B **77**, 165104 (2008).

[37] Y. Shinohara, K. Yabana, Y. Kawashita, J.-I. Iwata, T. Orobe, G. F. Berts, Phys. Rev. B **82**, 155110 (2010).

[38] D. Caldwell, Mol. Phys. **33**, 495 (1977).

[39] N. Troullier and J. L. Martins, Phys. Rev. B **43**, 1993 (1991).

[40] J. P. Perdew and A. Zunger, Phys. Rev. B **23**, 5048 (1981).

[41] Y. Kawashita, K. Yabana, M. Noda, K. Nobusada, T. Nakatsukasa, J. Mol. Struct.: THEOCHEM **914**, 130 (2009).

[42] B. P. Kafle, H. Katayanagi, Md. Serajul, I. Prodhan, H. Yagi, C. Huang, J. Phys. Soc. Jpn. **77**, 014302 (2008).

[43] H. Yagi, K. Nakajima, K. R. Koswattage, K. Nakagawa, C. Huang, Md. S. I. Prodhan, B. P. Kafle, H. Katayanagi, and K. Mitsuke, Carbon **47**, 1152 (2009).

[44] Z. Gasyna, P. N. Schatz, J. P. Hare, T. J. Dennis, H. W. Kroto, R. Taylor, D. R. M. Walton, Chem. Phys. Lett. **183**, 283 (1991).

[45] M. Pilch, M. Pawlikowski, and O. S. Mortensen, Chem. Phys. **172**, 277 (1993).

[46] K. Yabana and G. F. Bertsch, Phys. Rev. A **58**, 2604 (1998).

[47] P. Blöchl, Phys. Rev. B **50**, 17953 (1994).

[48] R. van Leeuwen and E. J. Baerends, Phys. Rev. A **49**, 2421 (1994).